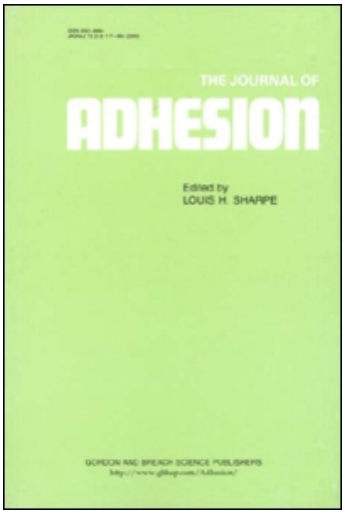

The Journal of Adhesion
Publication details, including instructions for authors and subscription information:
http://www.informaworld.com/smpp/title~content=t713453635

AXISYMMETRIC DROP SHAPE ANALYSIS (ADSA) FOR THE DETERMINATION OF SURFACE TENSION AND CONTACT ANGLE

M. Hoorfar[a]; A. W. Neumann[a]
[a] Department of Mechanical and Industrial Engineering, University of Toronto, Toronto, Ontario, Canada

Online publication date: 10 August 2010

To cite this Article Hoorfar, M. and Neumann, A. W.(2004) 'AXISYMMETRIC DROP SHAPE ANALYSIS (ADSA) FOR THE DETERMINATION OF SURFACE TENSION AND CONTACT ANGLE', The Journal of Adhesion, 80: 8, 727 — 743
To link to this Article: DOI: 10.1080/00218460490477684
URL: http://dx.doi.org/10.1080/00218460490477684

The Journal of Adhesion, 80: 727–743, 2004

ISSN: 0021-8464 print/1545-5823 online
DOI: 10.1080/00218460490477684

Taylor & Francis
Taylor & Francis Group

AXISYMMETRIC DROP SHAPE ANALYSIS (ADSA) FOR THE DETERMINATION OF SURFACE TENSION AND CONTACT ANGLE

M. Hoorfar
A. W. Neumann
Department of Mechanical and Industrial Engineering,
University of Toronto, Toronto, Ontario, Canada

A drop shape analysis technique called Axisymmetric Drop Shape Analysis (ADSA) has been developed in our laboratory over the last twenty years. ADSA is a powerful technique for the measurement of interfacial tensions and contact angles of pendant drops, sessile drops, and bubbles. In essence, it relies on the best fit between theoretical Laplacian curves and an experimental profile. Despite the general success of ADSA, deficient results may be obtained for drops close to spherical shape. Since the sources of these limitations were unknown, the entire ADSA technique, including hardware and software, has been reviewed. The key element of the new generation of ADSA is the modularization of the software, because a firm fixed package would not be suitable for all experimental situations. Another novel feature of the methodology is the development of a quantitative criterion, i.e., a shape factor, that determines the range of drop shapes, in which ADSA succeeds or fails.

Keywords: Surface tension; Image analysis; Numerical optimization; Shape Factor

Received 16 February 2004; in final form 6 April 2004.

One of collection of papers honoring A. W. Neumann, the recipient in February 2004 of *The Adhesion Society Award for Excellence in Adhesion Science, Sponsored by 3M*.

This work was supported by the Natural Science and Engineering Research Council (NSERC) of Canada under grant no. 8278. Financial support through an NSERC Postgraduate Scholarship (M. H) is gratefully acknowledged.

Address correspondence to A. W. Neumann, Department of Mechanical and Industrial Engineering, University of Toronto, 5 King's College Road, Toronto, Ontario, Canada M5S 3G8. E-mail: neumann@mie.utoronto.ca

INTRODUCTION

Thermodynamically speaking, in a solid–liquid system the work of adhesion can be expressed in terms of liquid surface tension and contact angle [1–3]. A methodology that can measure both is, therefore, an asset. Numerous methods have been developed for the measurement of contact angles and surface tensions of liquids [4]. Among all the methods, the pendant and sessile drop shape analysis methods have become the most widely used techniques. The determination of interfacial properties using drop shape analysis techniques is not based on an analytical solution and, therefore, involves a complicated numerical method. A number of computational procedures [5–9] have been developed for this purpose; axisymmetric drop shape analysis (ADSA) is versatile, powerful, and extensively used for the measurement of interfacial tensions and contact angles of pendant drops, sessile drops, and bubbles. In essence, it uses an efficient numerical scheme to fit a theoretical Laplacian curve with known surface tension values to an experimental profile obtained from a digital image of the drop. The next section of this article describes ADSA in detail. Some of the advantages of ADSA are (1) in comparison with other methods such as the Wilhelmy plate technique, much less liquid is required; (2) unlike the Langmuir film balance, ADSA can be used not only for insoluble but also for soluble films; and (3) in combination with suitable design and automation procedures, ADSA can act as a film balance by recording surface tension as a function of surface area of a drop, which is manipulated by changing the drop volume.

Despite the general success of ADSA, deficient results may be obtained, *e.g.*, for drops close to spherical shape. Since the source of this and possible other limitations were unknown, the entire ADSA technique including hardware and software has been reviewed. The hardware consists of optical, mechanical, and computer components that provide a digital image of the drop. The software consists of an image analysis process and a numerical method for the calculation of interfacial tension, contact angle, drop volume, and drop surface area.

AXISYMMETRIC DROP SHAPE ANALYSIS (ADSA)

The determination of interfacial properties from sessile and pendant drops involves a multistep process of image acquisition, image processing, and numerical computation. The image of the drop is acquired and transferred to a host computer using a microscope, a Charge-Coupled Device (CCD) monochrome camera, and a frame grabber (see Figure 1). A spot light source is used to illuminate the drop, and a heavily frosted diffuser

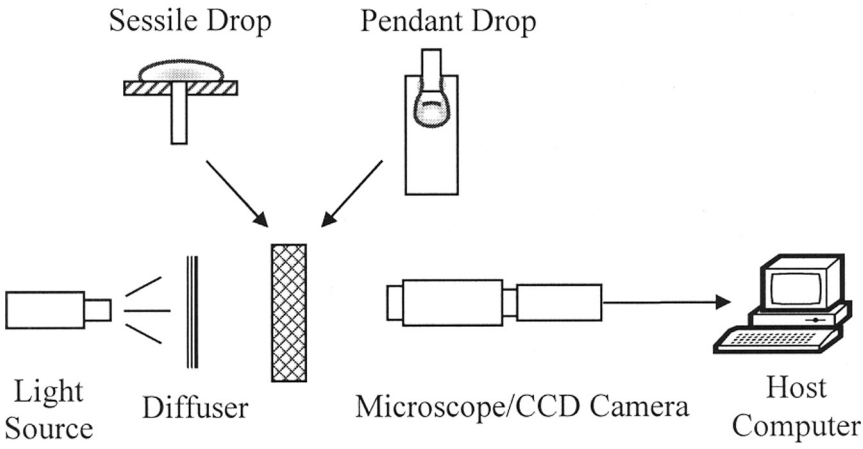

FIGURE 1 Schematic diagram of the experimental setup of ADSA for analysis of sessile and pendant drops.

is used in front of the light source to provide a uniformly lit background and to minimize heat emission to the drop during image acquisition.

An image analysis process (explained in the section below, "Image Analysis") has been employed to detect the coordinates of the drop profile. Finally, the measured profile of the drop is fitted to a Laplacian curve using an optimization method. The latter uses an objective function that specifies the discrepancy between the theoretical Laplacian curve and the actual profile as the sum of the squares of the normal distances between the measured points and the calculated curve. This objective function is minimized numerically to obtain the interfacial tension and contact angle values.

HARDWARE OF ADSA

The hardware consists of an image-digitizing board and optical components including a light source, microscope lens, and CCD camera. The performance of the image-digitizing board has been studied previously [10]. Below, the effects of the optical components on the performance of ADSA are scrutinized. It has been found that the range of light wavelengths, the lens aperture, and the CCD camera resolution have an impact on the results of ADSA, especially for near-spherical drops.

Light Source

A white light source was originally used to illuminate the pendant or sessile drops. Composed of a wide range of wavelengths, white light

forms chromatic effects such as rainbow and chromatic aberration that can cause blurring and loss of clearness of the edge of the drop [11–16]. These chromatic effects can be reduced using light with a narrow range of wavelengths. Therefore, a band-pass filter (*i.e.*, a filter that transmits wavelengths between the two cutoff wavelengths of the filter) can be used to pass only a narrow band of the visible wavelengths. The choice of an optical filter involves a tradeoff between the intensity and the bandwidth of light. In other words, the wider the bandwidth, the higher the intensity of light. An appropriate filter is expected to reduce the effect of chromatic aberration and the rainbow effect while maintaining sufficient intensity for the illumination.

The effect of different lighting conditions (*i.e.*, different optical filters with different ranges of wavelengths) has been investigated for different sizes of pendant drops. To obtain a wide range of drop sizes, the volume of the drop was changed continuously using a stepper motor. Figure 2 represents an example of the above experiment; it shows surface tension responses to changes of volume and surface area of a pendant drop of cyclohexane. Cyclohexane was chosen because it is a cyclic alkane and, hence, can be readily purified. The experiment was conducted using white light. The surrounding of the drop was maintained at 20°C. Since cyclohexane is a pure liquid (with purity greater than 99.9%), its surface tension is expected to remain constant regardless of the size of the drop. However, the results as determined by ADSA show that the surface tension value changes (in this case increases) as the surface area (or the volume) of the drop decreases (see Figure 2). Clearly, such findings must be erroneous. For a large drop with a well-deformed shape, *i.e.*, a drop with inflection points in the neck area, ADSA calculates the correct surface tension value, *i.e.*, the well-known value of the surface tension of cyclohexane (25.24 mJ/m^2 at 20°C) [17]. As the drop volume decreases, the drop shape becomes closer to spherical and the results start deviating from the correct value. This error is due to the limitations of ADSA in the determination of the surface tension of near-spherical drop shapes.

The above experiment was repeated using different optical filters (with different ranges of wavelengths). The results of these experiments are summarized in Table 1. It is clear that for the sufficiently large and, hence, well-deformed drop ADSA yields the correct surface tension value for all lighting conditions. On the other hand, for the small drops, various lighting conditions yield different results that differ from the literature value. The results also show that the use of any optical filter (red, green, or blue) reduces the discrepancy between the surface tension values obtained for large and small drops. This may be explained by the fact that filters reduce the chromatic

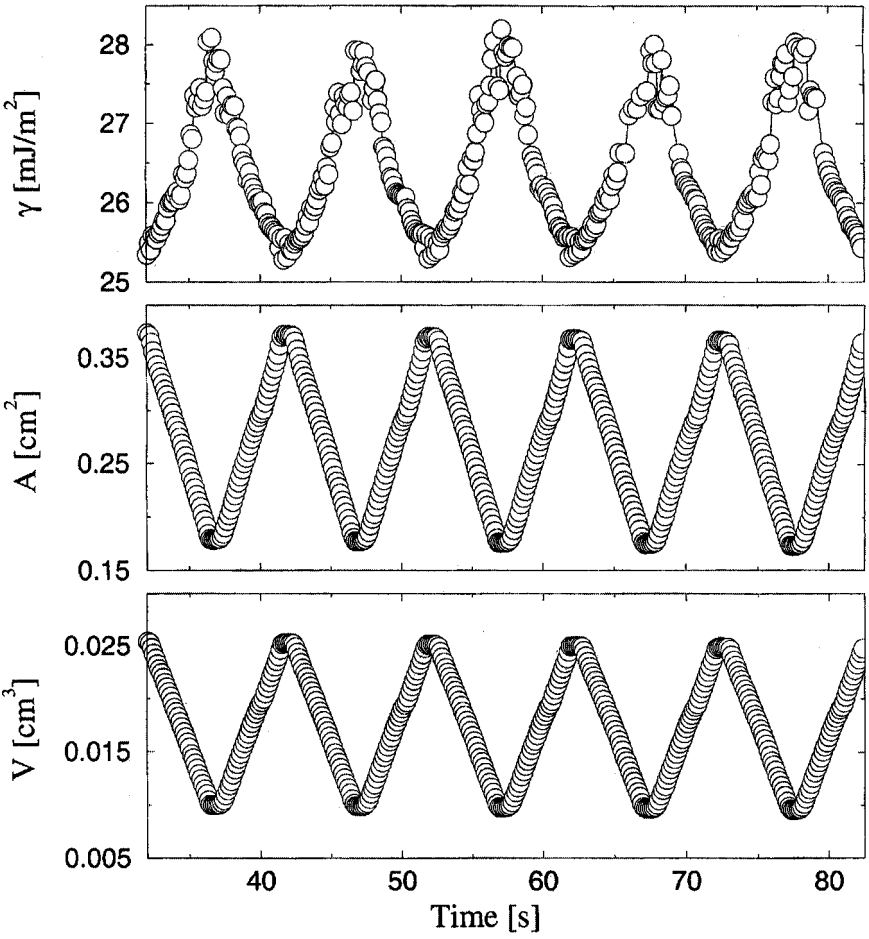

FIGURE 2 Surface tension responses to change of surface area of a pendant drop of cyclohexane in a dynamic cycling experiment (at 20°C) using white light.

effects caused by white light, so they improve the quality of the image. It is noted that the use of filters could reduce the intensity of light to a level at which ADSA cannot function properly. Thus, it may become necessary to boost the light source according to the bandwidth of the filter used. Finally, the results in the last column of Table 1 suggest that the Mikkle blue filter (with a wavelength range of 400–500 nm) is, as expected, the most effective filter among those tested. This result is in agreement with the laws of elementary optics [11].

TABLE 1 Surface Tensions of Large Drops (v = 26 μl) and Small Drops (v = 10 μl) Obtained from the Cycling Experiment Using Different Filters

White light +●●●	Wavelength range (nm)	γ (mJ/m^2) for large drop	γ (mJ/m^2) for small drop
No filter	390–720	25.23 ± 0.03	27.79 ± 0.31
Light red*	600–700	25.23 ± 0.03	27.44 ± 0.27
Velvet green*	450–550	25.23 ± 0.03	27.23 ± 0.20
Mikkle blue*	400–500	25.24 ± 0.03	26.89 ± 0.16

*These are commercial names for the filters purchased from LEE Filters Company (Toronto, Ontario, Canada)

Lens

Geometrical distortion and spherical aberration are the most significant problems of a lens in an optical system regardless of the type of illumination used (white light or monochromatic) [13]. Spherical aberration is caused by the failure of a lens to bring parallel rays of light into a single focus. Typically, the center and edges of a spherical lens have different focal points so that the images of objects, as seen through the whole surface of the lens, may be blurry. A simple way to alleviate the effect of the spherical aberration is to step down the aperture and use only the center of the lens. However, this will increase the depth of field, which is not desired in this application because the image processing module requires a distinct image focused at the meridian plane. From this point of view, it is preferable to open the aperture as wide as possible, which will increase the spherical aberration. In general, a compromise between these conflicting requirements may have to be found. In our setup an apochromatic lens (*i.e.*, a series of lenses arranged in a row to reduce spherical aberration) is used, which minimizes the spherical aberration and, thus allows us to open the aperture fully. Table 2 summarizes the

TABLE 2 Surface Tensions of Large Drop (v = 26 μl) and Small Drop (v = 10 μl) Obtained from the Cycling Experiment Using Two Different Choices of Aperture

Aperture	γ (mJ/m^2) for large drop	γ (mJ/m^2) for small drop
Fully open	25.23 ± 0.03	27.79 ± 0.31
Partially open	25.31 ± 0.17	28.03 ± 0.45

TABLE 3 Surface Tensions of Large Drop ($v = 26\,\mu l$) and Small Drop ($v = 10\,\mu l$) Obtained from the Cycling Experiment Using High and Low Resolution Cameras

Image resolution (pixel × pixel)	γ (mJ/m^2) for large drop	γ (mJ/m^2) for small drop
High (1280 × 960)	25.24 ± 0.03	26.93 ± 0.18
Low (640 × 480)	25.23 ± 0.03	27.79 ± 0.31

surface tension values of cyclohexane measured with two choices of aperture, *i.e.*, fully open and partially open, in the cycling experiment described before. The results show that the discrepancy between the surface tension values obtained for large and small drops is smaller when the aperture is fully open.

In order to avoid the effect of geometrical distortion, a software module was incorporated into the first generation of ADSA to eliminate the effect of the optical distortion of the lens using a calibration grid pattern engraved on an optical glass slide (see the section below, "Image Analysis") [18, 19].

CCD Camera

The resolution of the camera has an impact on the quality of the image acquired. Assuming that the other parameters of the system are perfect, the edge detection error due only to the resolution of the camera is expected to be about the size of a pixel. Thus, the lower the resolution (or the larger the size of the pixels) the larger the errors in the edge of the drop.

Several experiments have been conducted with different image resolutions. Table 3 summarizes the surface tension value of cyclohexane measured with two different camera resolutions in the cycling experiment described before. It is clear that the higher the resolution of the image (*e.g.*, 1280×960 pixels), the smaller the difference between the surface tension values of large and small drops. In other words, the higher resolution camera produces higher quality images that improve the accuracy of the results.

SOFTWARE OF ADSA

Image Analysis

The first part of the software is the image-processing technique that detects the edge of the drop automatically [18, 19]. It consists of four

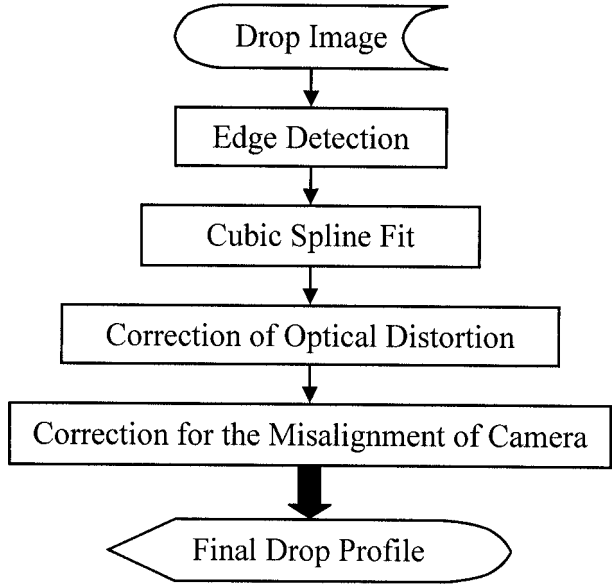

FIGURE 3 Flowchart of the four steps of the image analysis part of ADSA.

steps as shown in Figure 3. First, the edge of the drop is obtained using the Sobel edge operator [18–23], whose output has high magnitude at the pixels where the gray levels are changing rapidly, *i.e.*, at the edge. In this stage, the edge is a discrete curve in which the minimum distance between two adjacent points is equal to the size of a pixel. To achieve higher accuracy, the edge is smoothened using a cubic spline technique to provide subpixel resolution. Then, the edge is corrected by means of a calibration grid to eliminate the effect of the optical distortion caused by the microscope lens. Finally, the misalignment of the camera with respect to the true vertical line as given by a plumb line is corrected by means of an appropriate transformation matrix [18].

In the previous generation of ADSA, the components of the image-analysis process were mixed so that the study of the effect of each component, as well as further improvements, was difficult, if not impossible. Therefore, the image analysis part has been redeveloped in a fully modular form so that the significance of each module in the performance of ADSA can be evaluated separately. Table 4 shows the effect of each step of the image analysis part of ADSA for a large pendant drop of cyclohexane. Each column of the table includes (1) the average of the surface tension values of the largest drops in ten

TABLE 4 Surface Tension Values of Cyclohexane Obtained as Each Step of Image Analysis Part Was Added to the Previous Steps

Image analysis steps	Sobel edge detection	Cubic spline fit	Optical distortion correction	Camera misalignment correction
γ (mJ/m^2)	26.36 ± 0.15	26.23 ± 0.08	25.47 ± 0.03	25.23 ± 0.03

cycles, and (2) the error limits obtained based on the standard deviation of the surface tension values in ten cycles with a 95% confidence level. It is clear that as each step is taken the surface tension value approaches the correct value and the error significantly decreases.

With the image analysis part of ADSA now being modular, it is possible to compare different edge-detection techniques with the Sobel edge operator used by previous generations of ADSA. Table 5 summarizes the surface tension values of a large drop of cyclohexane obtained using different edge detection methods in two different conditions: (1) with drop profile corrections (*i.e.*, cubic spline fitting technique, optical distortion correction, and misalignment correction of camera), and (2) without drop profile corrections. It is clear that the drop profile corrections have a considerable impact on the consistency of the results no matter which edge detection method is used.

Finally, the performance of ADSA for large and small drops has been compared using different edge detection techniques. Table 6 shows the effect of different edge techniques on the surface tension values of cyclohexane for small and large drops. The results reveal that the effect of different edge detection techniques is significant for the small drop. The Canny method [24] may have particular merit, as the deviation between the surface tension values obtained for small and large drops is smaller than the values obtained using other edge detection techniques. The improvement of the results is possibly due

TABLE 5 Surface Tension Values Obtained with and without Drop Profile Corrections Using Different Edge Detections

Edge detection	With drop profile corrections, γ (mJ/m^2) for large drop	Without drop profile corrections, γ (mJ/m^2) for small drop
Sobel	25.23 ± 0.03	26.36 ± 0.15
Roberts	25.23 ± 0.03	26.38 ± 0.16
Prewitt	25.23 ± 0.03	26.37 ± 0.14
LOG	25.23 ± 0.03	26.62 ± 0.11
Canny	25.23 ± 0.03	26.26 ± 0.11

TABLE 6 Surface Tension Values Obtained Using Different Edge Detections for Small and Large Drops of Cyclohexane

Edge detection	γ (mJ/m^2) for large drop	γ (mJ/m^2) for small drop
Sobel	25.23 ± 0.03	27.79 ± 0.31
Roberts	25.23 ± 0.03	27.87 ± 0.43
Prewitt	25.23 ± 0.03	27.78 ± 0.30
LOG	25.23 ± 0.03	27.48 ± 0.22
Canny	25.23 ± 0.03	27.17 ± 0.18

to the fact that Canny edge detection removes noise from the image using a convolution Gaussian filter prior to the edge detection and uses two different threshold values for "strong" and "weak" edges [20].

Numerical Scheme

The second part of the software is the numerical scheme. In the first generation of ADSA, Rotenberg *et al.* [25, 26] introduced a versatile numerical methodology for the measurement of interfacial properties. However, the algorithm has convergence problems for flat sessile drop shapes, *e.g.*, for small surface tensions. Therefore, del Río *et al.* [27] developed a second generation of ADSA to overcome certain deficiencies of the original numerical method, using more efficient algorithms. A thorough investigation was carried out to compare the performance of the two algorithms. A theoretical drop shape (Laplacian curve) with 8 significant figures for each coordinate point (shown in Figure 4a) was generated using an appropriate program called Axisymmetric Liquid-Fluid Interfaces (ALFI) [28]. For all intents and purposes, this profile is perfect and comparable with a hypothetical experimental profile obtained with an accuracy of 0.1 nm. Surface tension values at different cutoff levels (see Figure 4a), starting from the neck to the apex, were obtained using the two ADSA methods. At the "starting cutoff level" shown in Figure 4a, the drop profile is called a well-deformed drop since it has inflection points (in the neck area). For the well-deformed drop profile the two ADSA algorithms give the correct surface tension value, say to six significant places, *i.e.*, well beyond any possible experimental accuracy. As the cutoff level is placed lower and lower, it becomes apparent that the del Río algorithm is more stable than the Rotenberg algorithm. Generally, the Rotenberg algorithm fails in certain situations where the del Rió algorithm works properly. Finally, the second generation (del Río) ADSA also fails, although not as easily, as the drop shape near the

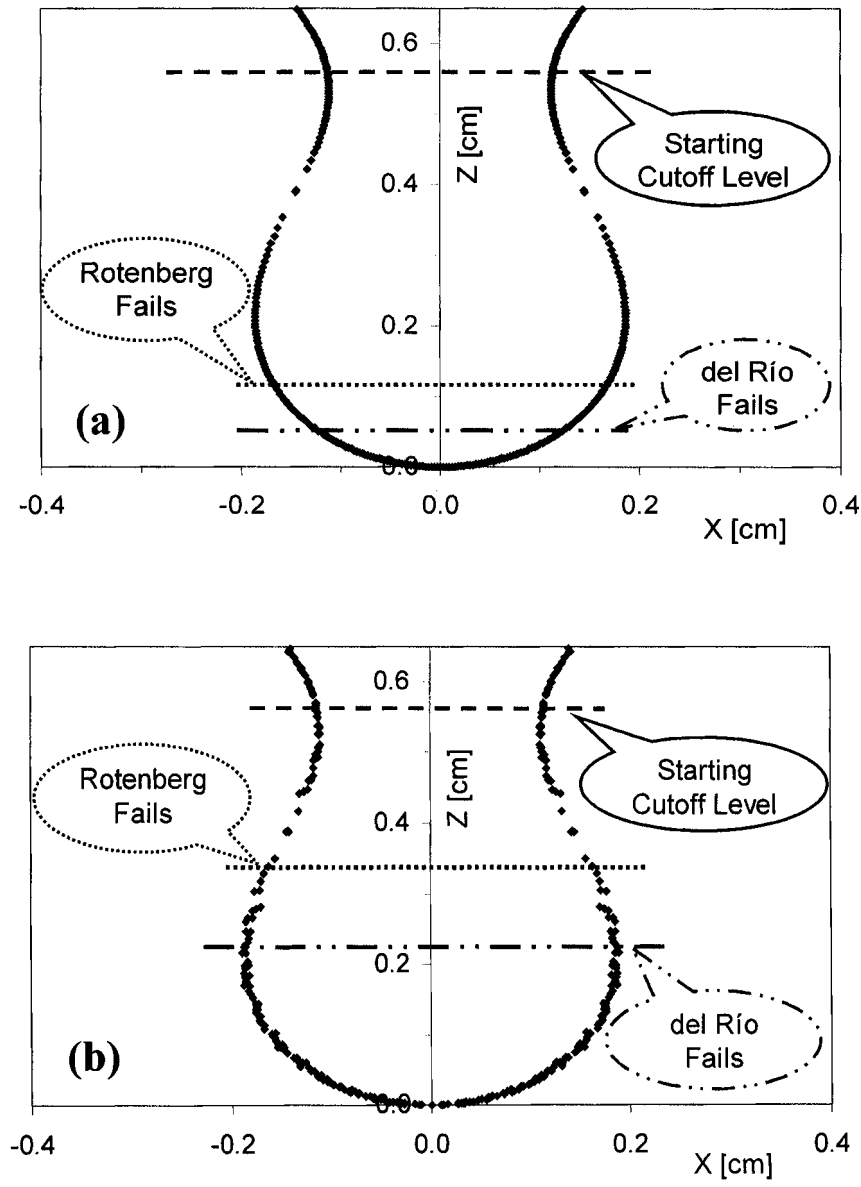

FIGURE 4 (a) Performance of the two ADSA algorithms at different cutoff levels for a theoretical drop profile generated with 8 significant figures for each coordinate point. (b) Performance of the two ADSA algorithms at different cutoff levels for a theoretical drop profile perturbed randomly by the equivalent of one pixel.

apex becomes indistinguishable from spherical. To mimic the performance of the two algorithms in real experimental situations, the ideal drop profile was perturbed randomly by the equivalent of one pixel, *i.e.,* a reasonable estimate for the experimental error in the acquisition of a real drop image. Figure 4b shows the perturbed theoretical drop profile that mimics the experimental errors. It is apparent from Figure 4b that the two algorithms fail sooner for the perturbed profile than for the ideal profile shown in Figure 4a. It can be expected that in the real experimental situation, where the drop profile is obtained with a smaller number of significant figures, the two algorithms fail sooner compared with the above two cases (Figures 4a and 4b).

The limitation of the numerical scheme for the near-spherical drops is due to accumulation of round-off errors that may be the ultimate limitation of all numerical schemes. Theoretically, each drop shape corresponds to a certain surface tension value. For nearly spherical drop shapes, significantly different surface tension values correspond to only slightly different drop shapes so that the numerical solver can easily become unstable due to truncation errors. More precisely, truncation errors cause dramatic output changes due to a small variation of inputs which impacts on efficiency and stability of the numerical scheme. In view of the above limitation of the ADSA algorithm, it is necessary to develop a quantitative criterion to determine the quality of the surface tension measurements obtained from ADSA for different drop shapes.

Shape Factor

The results in the previous tables show that the surface tension values obtained from ADSA for near-spherical drops are still different from the correct values even after improving the hardware and the use of more sophisticated edge-detection techniques. Therefore, it is necessary to develop a quantitative criterion that determines the range of drop shapes in which ADSA succeeds or fails. For this purpose, we have developed a shape factor that expresses quantitatively the difference in shape between a given experimental drop and a spherical shape. Such a factor is formulated using the fact that the curvature along the periphery of a spherical drop, is constant, whereas it changes markedly for a well-deformed drop. The shape factor is defined as

$$P = \frac{1}{\pi R_0^2} \int_0^{2\pi} \int_0^{r} r dr d\theta - 1, \tag{1}$$

where R_0 is the radius of the curvature at the apex.

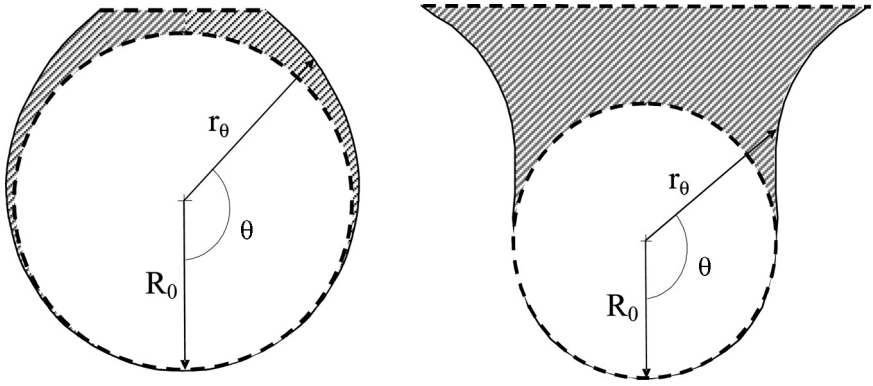

FIGURE 5 The shape factor that refers to the hatched area between the drop profile and a circle with a radius of R_0.

The shape factor refers to the hatched area between the drop profile and a circle with a radius of R_0, which is the radius of the curvature at the apex given by ADSA (see Figure 5). The shape factor has been normalized based on the area of the circle to eliminate the effect of size of the image or magnification. It is noted that the shape factor is greater for the well-deformed drops than for the near-spherical drops.

To investigate the relationship between the shape factor and the performance of ADSA, an auxiliary program has been developed to calculate shape factors corresponding to different surface tension values obtained for a range of drop profiles with different drop volumes. Figure 6 shows two different drops of cyclohexane and the corresponding shape factors.

Figure 7 shows the variation of the surface tension values *versus* the shape factors calculated for the above cycling experiment of cyclohexane. A surface tension relative error, ε_{rel}, was defined as the difference between the surface tension value obtained from ADSA for each drop size and the surface tension value obtained from ADSA for the well-deformed drop, *i.e.*, the true surface tension. The relative error is also normalized based on the surface tension value obtained for the well-deformed drop. The surface tension relative error ε_{rel} is given by

$$\varepsilon_{rel} = \frac{\gamma}{\bar{\gamma}_{wd}} - 1, \tag{2}$$

where $\bar{\gamma}_{wd}$ is the average surface tension value for the well-deformed drops obtained from different cycles.

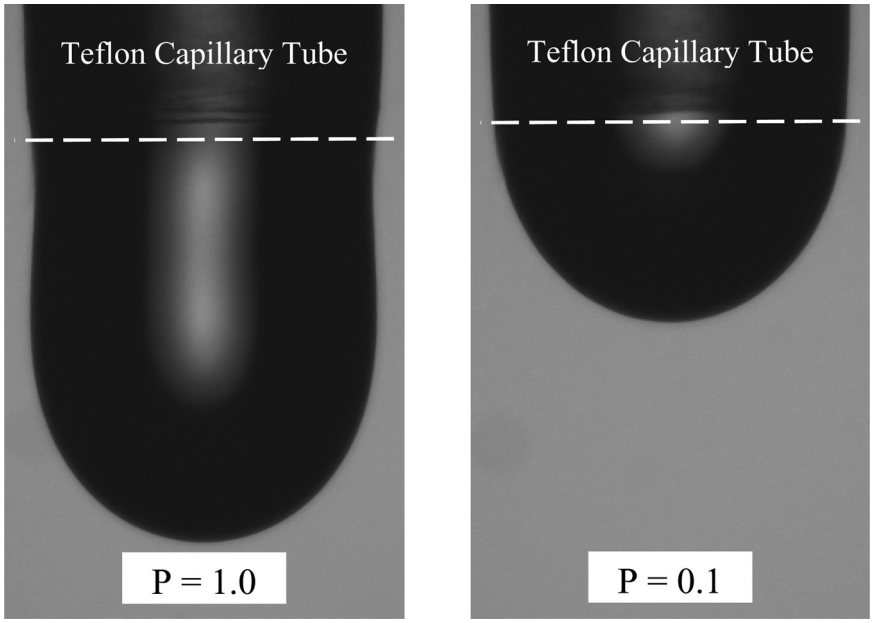

FIGURE 6 Shape factors of the two different drop sizes.

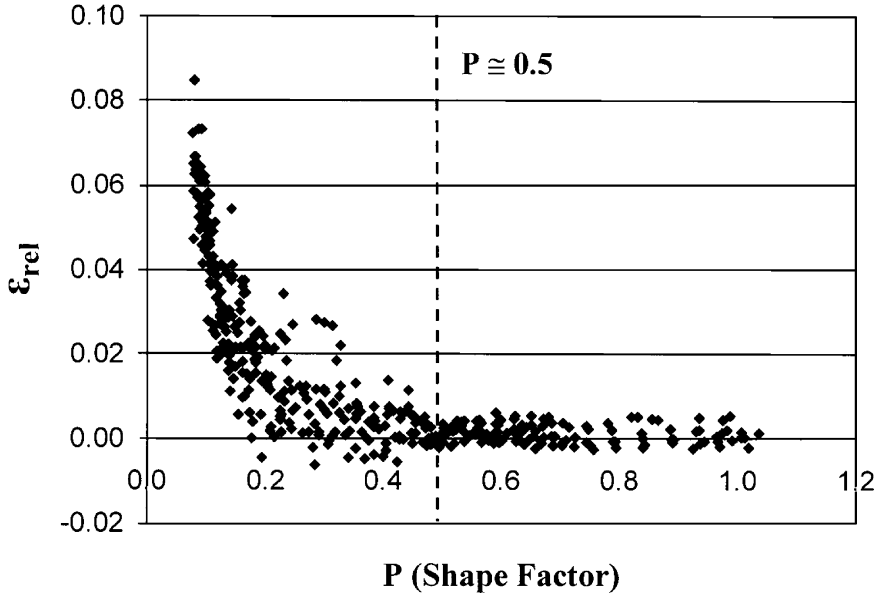

FIGURE 7 Surface tension relative errors *versus* shape factors.

The relative error is plotted over the shape factor in Figure 7. The graph is divided into two parts. For large shape factors, $P \geq 0.5$, the relative error is relatively constant near zero and bounded, verifying that ADSA performs accurately in this part, *i.e.*, for well-deformed drops. Thus, drop profiles with shape factors of 0.5 or higher may be used for surface tension measurements. On the other hand, for small shape factors, $P < 0.5$, the relative error grows rapidly with the decrease of the shape factor so that the accuracy of ADSA deteriorates significantly. The threshold of 0.5 in this experiment may be referred to as the critical shape factor (*i.e.*, $P_{cr} = 0.5$). It is noted that the use of the shape factor introduces a quantifiable meaning for the large and well-deformed drops that can estimate the performance of ADSA up front. Since the shape factor is a parameter that solely depends on the geometry of the drop, it is expected that the critical shape factor and its pattern shown in Figure 7 is more or less invariant from one liquid to another, but not necessarily from one drop shape to another. Therefore, a range of the shape factors of different drop shapes for both pendant and sessile drops has to be calculated and explored to (1) specify the circumstances under which ADSA performs flawlessly, *i.e.*, $P \geq P_{cr}$, and (2) determine a confidence level for the surface tension values corresponding to small shape factors, $P < P_{cr}$.

The shape factor can be a useful criterion in situations where it is not possible to avoid drop shapes approaching spherical shape. To stay with the example of ADSA as a film balance, we observe in many instances very interesting patterns at high compression, *i.e.*, necessarily for small, and hence relatively spherical, drops. However, we must be able to exclude possible ADSA artifacts before interpreting such patterns, which may not be obtainable with other methodologies. The shape factor can be used to estimate the quality of the surface tension determination in such experiments.

SUMMARY

The hardware and software of ADSA have been scrutinized. The progress toward the development of the new generation of ADSA is summarized as follows:

- The effect of optical filters on the performance of ADSA has been studied. Reducing the chromatic effects caused by white light, the optical filters improve the quality of the images acquired and consequently the results obtained from ADSA, especially for near-spherical drops. Also, it has been shown that a blue filter (with the wavelength range of 400−500 nm) is particularly effective.

- The choice of the aperture and the resolution of the camera has also been examined. It has been found that the aperture must be fully open to minimize the depth of focus to facilitate acquisition of a drop image at the meridian plane. A high-resolution camera is recommended to produce a high-quality image.
- The image analysis package of ADSA has been redeveloped in a modular form so that the significance of each module in the performance of ADSA can be evaluated separately. As a result, we were able to test a variety of state-of-the-art edge-detection techniques and compare them with the Sobel edge-detection technique that was originally used. The results of several experiments show that the effect of different edge-detection techniques is significant, especially for small drops. The results also suggest that among all edge detection methods the so-called Canny methodology yields the most accurate results.
- A thorough investigation was carried out to compare the performance of the two algorithms of ADSA, *i.e.*, the Rotenberg algorithm and the del Río algorithm. The results show that the second generation of ADSA, which is superior to the first algorithm, ultimately fails for drops close to spherical shapes. The limitation is due to accumulation of round-off errors, which may be the ultimate limitation of all numerical schemes.
- A shape factor was developed to determine the range of drop shapes in which ADSA succeeds or fails. In essence, it expresses quantitatively the difference in shape between a given experimental profile and a spherical shape. The shape factor has been calibrated with drops of known surface tension values ranging from well-deformed shapes to near-spherical shapes. A critical shape factor has been obtained based on the results of the preliminary experiments. The shape factors above the critical shape factor, *i.e.* 0.5, guarantee the validity of the surface tension determination.

REFERENCES

[1] Wu, S., In: *Polymer Interface and Adhesion* (Marcel Dekker, Inc., New York and Basel, 1982), Chap. 11, pp. 360–370.
[2] Norde, W., In: *Colloids and Interfaces in Life Science* (Marcel Dekker, Inc., New York and Basel, 2003), Chap. 5, pp. 70–72.
[3] Hiemenz, P. C., In: *Principles of Colloid and Surface Chemistry*, 2nd ed. (Marcel Dekker, Inc., New York and Basel, 1986), Chap. 6, pp. 314–322.
[4] Adamson, A. W., In: *Physical Chemistry of Surface*, 5th ed. (John Wiley and Sons, New York, 1990), Chap. 2, pp. 9–44.
[5] Bashforth, F. and Adams, J. C., In: *An Attempt to Test the Theory of Capillary Action by Comparing the Theoretical and Measured Forms of Drops of Fluid*

(Cambridge University Press and Deighton Bell & Co., Cambridge, 1892), Chap. 3, pp. 13–56.
[6] Hartland, S. and Hartley, R. W., In: *Axisymmetric Fluid-Liquid Interfaces* (Elsevier, Amsterdam, 1976), pp. 514–722.
[7] Maze, C. and Burnet, G., *Surface Sci*. **13**, 451–470 (1969).
[8] Maze, C. and Burnet, G., *Surface Sci*. **24**, 335–342 (1971).
[9] Anastasiadis, S. H., Chen, J. K., Koberstein, J. T., Siegel, A. P., Sohn, J. E., and Emerson, J. A., *J. Colloid Interface Sci*. **119**, 55–66 (1986).
[10] Hoorfar, M., In: *Development of a PC Version for Axisymmetric Drop Shape Analysis (ADSA)*, University of Toronto, M.A.Sc. Thesis, 2001, Chap. 5, pp. 59–68.
[11] Hecht, E., In: *Optics*, 3rd. ed. (Addison-Wesley Pub. Co., 1987), pp. 257–284.
[12] Smith, W., In: *Optical Engineering: The Design of Optical Systems* (McGraw-Hill, New York, 2000), pp. 61–90.
[13] Rutten, H., van Venrooij, M., In: *Telescope Optics: Evaluation and Design*, R. Berry, Ed. (Willmann-Bell, Inc., Richmond, VA., U.S.A., 1988), Chap. 4, pp. 19–42.
[14] Guo, K. H., Uemura, T., and Yang, W., *Appl. Opt.* **24**, 2655–2659 (1985).
[15] Thomas, L. P., Gratton, R., Marino, B. M., and Diez, J. A., *Appl. Opt.* **34**, 5840–5848 (1995).
[16] Chan, C. K., Liang, N. Y., and Liu, W. C., *Rev. Sci. Instrum*. **64**, 632–637 (1993).
[17] Jasper, J. J., *J. Phys. Chem. Ref. Data* 1(3), 856–857 (1972).
[18] Cheng, P., *Automation of Axisymmetric Drop Shape Analysis Using Digital Image Processing*, University of Toronto, Ph.D. Thesis, 1990, pp. 61–158.
[19] Cheng, P., Li, D., Boruvka, L., Rotenberg, Y., and Neumann, A.W., *Colloids Surf.*, **43**, 151–167 (1990).
[20] Castleman, K. R., In: *Digital Image Processing* (Prentice-Hall, Englewood Cliffs, NJ, 1979), pp. 58–135.
[21] Pratt, W. K., In: *Digital Image Processing*, 3rd ed. (Wiley-Interscience, New York, 1978) Chap. 15, pp. 443–508.
[22] Ekstrom, M. P., In: *Digital Image Processing Techniques* (Academic Press Inc., Orlando, FL, 1984), Chap. 7, pp. 257–286.
[23] Davis, L. S., *Comp. Graphics Image Proc.* **4**, 248–270 (1975).
[24] Canny, J., *IEEE Trans. Pattern Anal. Machine Intell.* **8**(6), 679–698 (1986).
[25] Rotenberg, Y., *The Determination of the Shape of Non-Axisymmetric Drops and the Calculation of Surface Tension, Contact Angle, Surface Area and Volume of Axisymmetric Drops*, University of Toronto, Ph.D. Thesis 1983, Chaps. 8–12.
[26] Rotenberg, Y., Boruvka, L., and Neumann, A. W., *J. Colloid Interface Sci.* **93**, 169–183 (1983).
[27] del Rio, O. I., *On the Generalization of Axisymmetric Drop Shape Analysis*, University of Toronto, M.A.Sc. Thesis, 1993, Chap. 3, pp. 24–40.
[28] del Rio, O. I. and Neumann, A. W., *J. Colloid Interface Sci.* **196**, 136–147 (1997).